Microbunch Rotation and Coherent Undulator Radiation from a Kicked Electron Beam

James P. MacArthur,[1,2,*] Alberto A. Lutman,[1] Jacek Krzywinski,[1] and Zhirong Huang[1,2,†]
[1]*SLAC National Accelerator Laboratory, Menlo Park, California 94025, USA*
[2]*Stanford University, Stanford, California 94305, USA*

(Received 17 April 2018; revised manuscript received 9 August 2018; published 29 November 2018)

Coherent emission from a microbunched electron beam is the driving force behind the revolution in light sources, enabling x-ray free-electron lasers (FELs) to emit pulses 9 orders of magnitude brighter than previous sources. Microbunches form perpendicular to the electron travel direction, and the conventional understanding is that they shear rather than rotate in response to a transverse kick, locking FEL facilities into a single-user operating mode. In this paper, we show that microbunches rotate toward the new direction of travel if the electron beam is kicked and defocused. We provide evidence that microbunch rotation explains the unexpectedly large amount of off-axis radiation observed during experiments at the Linac Coherent Light Source. We demonstrate that LCLS can be multiplexed into at least three separate beams using this principle. Finally, we propose using a magnetic triplet to rotate microbunches through significantly larger angles without microbunch degradation. This new understanding of microbunch dynamics can lead to significantly improved multiplexing at FEL facilities, microbunch preservation through a bend, and x-ray pulses with a pulse-front tilt.

DOI: 10.1103/PhysRevX.8.041036 Subject Areas: Atomic and Molecular Physics, Optics

I. INTRODUCTION

The unprecedented brightness and coherence of x-ray free-electron lasers (FELs) has enabled new research in physics, chemistry, and biology at the characteristic length and timescales of atomic and molecular phenomena [1,2]. The flexibility and maturity of particle-beam manipulation has been leveraged to produce customized x-ray pulses for users of x-ray FEL facilities [3–10]. Sometimes, however, our understanding of electron and radiation interactions are pushed into unfamiliar territory.

One such situation arose during the commissioning of the arbitrary polarization Delta undulator at the Linac Coherent Light Source (LCLS). A premicrobunched electron beam was given a transverse kick immediately before the Delta undulator. This produced an angular separation between the background linearly polarized x-ray pulse and the circularly polarized x-ray pulse from the Delta undulator [11]. This technique leads to nearly 100% circularly polarized soft x rays at LCLS [12,13].

With a carefully chosen undulator K parameter in the Delta undulator, a powerful diverted beam was observed at several times the intrinsic beam divergence. It is generally understood that a transverse kick does not change the microbunch orientation, and hence suppresses the coherent radiation emitted in the direction of the electron motion [14,15]. This understanding has been formalized into a theory of far-field radiation from a kicked beam [16,17], but is inconsistent with Delta undulator experiments.

Recently, another explanation has been offered, that the conventional theory of radiation from charges is inconsistent with relativity, and that "the orientation of the microbunching wave front in the ultrarelativistic asymptotic is always perpendicular to the electron beam velocity" [18–20]. Such an effect would aid in the production of off-axis radiation.

In the following section we begin with the conventional viewpoint that the microbunch angle is not immediately affected by a transverse kick. We depart from the standard theory and find that microbunch rotation develops as a consequence of quadrupole focusing, as illustrated in Fig. 1. Rotation is shown to enable more efficient off-axis lasing, matching numerical simulations and experimental results. We conclude with a demonstration of applications for this effect, including the potential for significant improvement in multiplexing at soft and hard x-ray FEL facilities, microbunch preservation through hundreds of microradians of bend, and x-ray beams with a pulse-front tilt.

*jmacart@slac.stanford.edu
†zrh@slac.stanford.edu

II. MICROBUNCH ROTATION IN A FOCUSING CHANNEL

Corrector dipole magnets are integrated into the undulator lattice quadrupoles at LCLS. The corrector immediately upstream of the Delta undulator can be used to divert a microbunched beam vertically. This situation is depicted in Fig. 1. In this section we calculate the microbunch tilt $\alpha_b(z)$. We do so with an eye toward calculating the far-field radiation distribution in the following section.

The dynamics of a beam of N_e electrons moving in a helical undulator are described by the Klimontovich distribution function

$$\mathcal{F} = \frac{k_1}{I/ec}\sum_{j=1}^{N_e}\delta(\theta-\theta_j)\delta(\eta-\eta_j)\delta(\mathbf{x}-\mathbf{x}_j)\delta(\mathbf{x}'-\mathbf{x}'_j),$$

where j indexes each electron, $\theta_j = (k_1+k_u)z_j - \omega_1 t$ is the ponderomotive phase, $k_1 = \omega_1/c$ is the wave number resonant to the helical undulator $k_u = 2\pi/\lambda_u$, with λ_u representing the undulator period, $\eta_j = (\gamma_j-\gamma_r)/\gamma_r$ is the energy relative to the resonant electron energy γ_r, $\mathbf{x}_j$ is the transverse position in the (x,y) plane, and $\mathbf{x}'_j = d\mathbf{x}_j/dz$ is the transverse momentum. $\mathcal{F}$ is normalized by the current I.

$\mathcal{F}$ can be decomposed into a background, stationary distribution $\bar{F}$, and microbunched perturbation F that contains FEL induced modulation, $\mathcal{F} = \bar{F} + F$. At a particular frequency $\nu = k/k_1$, the interaction between the field $E_\nu(\mathbf{x};z)$ and the perturbation distribution $F_\nu(\mathbf{x},\mathbf{x}',\eta;z) = \int e^{-i\nu\theta}F d\theta$ is described by the linearized Maxwell-Klimontovich equations [21],

$$\left[\frac{\partial}{\partial z} + i\Delta\nu k_u + \frac{ik}{2}\boldsymbol{\phi}^2\right]\tilde{E}_\nu = -\kappa_1 n_e\int d\mathbf{x}' d\eta \tilde{F}_\nu, \quad (1)$$

$$\left[\frac{d}{dz} + i\left(2\nu\eta k_u - \frac{k}{2}\mathbf{x}'^2\right)\right]F_\nu = -\chi_1 E_\nu\frac{\partial\bar{F}}{\partial\eta}, \quad (2)$$

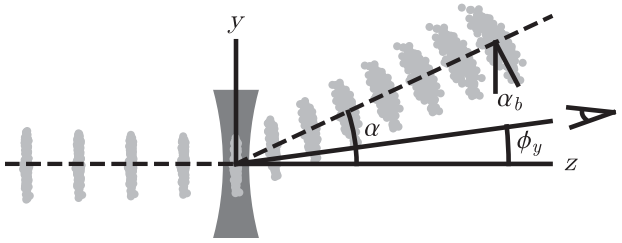

FIG. 1. Microbunched electrons (light gray) traveling left to right along the z axis are kicked by an angle α in the $+y$ direction. The microbunches acquire an automatic tilt angle α_b as a result of the defocusing quadrupole (dark gray) at $z=0$. Microbunch smearing and curvature are also present. An observer in the far field sits at an angle ϕ_y above the z axis.

where the tilde indicates an angular transform,

$$\tilde{E}_\nu(\boldsymbol{\phi};z) = \frac{1}{\lambda^2}\int d\mathbf{x}E_\nu(\mathbf{x};z)e^{-ik\mathbf{x}\cdot\boldsymbol{\phi}},$$
$$\tilde{F}_\nu(\boldsymbol{\phi},\boldsymbol{x}',\eta;z) = \frac{1}{\lambda^2}\int d\mathbf{x}F_\nu(\mathbf{x},\boldsymbol{x}',\eta;z)e^{-ik\mathbf{x}\cdot\boldsymbol{\phi}},$$

$\chi_1 = eK/\sqrt{2}\gamma_r^2 mc^2$, $\kappa_1 = eK/2\sqrt{2}\epsilon_0\gamma_r$, n_e is the electron volume density, K is the helical undulator strength parameter, ϵ_0 is the vacuum permittivity, and $\Delta\nu = \nu - 1$. The d/dz on the left side of Eq. (2) is a total derivative along the trajectory, and the natural focusing of the helical undulator is ignored because it is much weaker than quadrupole focusing in an x-ray FEL.

We will solve Eqs. (1) and (2) for the situation depicted in Fig. 1. The transverse position of a given electron for $z \geq 0$ is [22]

$$x(z) = x_0 + (x'_0 - x_0/2f)z, \quad (3)$$

$$y(z) = y_0 + (y'_0 + y_0/2f + \alpha)z, \quad (4)$$

where f is the signed focal length of the quadrupole, α is the dipole kick, and $z=0$ corresponds to the center of the quadrupole. At LCLS the kick is generated inside the quadrupole, but a kick generated by a nearby dipole would be sufficient. A positive focal length represents a quadrupole that is defocusing in the y dimension. Previous treatments implicitly set $|f| = \infty$.

It is instructive to calculate the difference in longitudinal position between a sample electron and the dashed reference trajectory of Fig. 1,

$$\begin{aligned}\Delta\ell &\approx z\cos(y'_0 + y_0/2f + \alpha) - z\cos\alpha \\ &\approx \frac{\alpha z}{2f}y_0 + \alpha z y'_0 + \frac{z}{2}\left(\frac{1}{2f}y_0 + y'_0\right)^2, \end{aligned} \quad (5)$$

where we have expanded to second order. The first term is a linear correlation between $\Delta\ell$ and y, or tilt. When $y \approx y_0$, the tilt is $\alpha_b = d\ell/dy \approx d\ell/dy_0 \approx \alpha z/2f$. The second and third terms represent microbunch smearing, curvature, and other detrimental correlations. A rigorous calculation of α_b for $y \approx y_0$ follows.

The electron beam in an FEL is confined by a focusing-drift-defocusing-drift (FODO) lattice, wherein $\langle x_0\rangle = \langle y_0\rangle = \langle x'_0\rangle = \langle y'_0\rangle = \langle x_0x'_0\rangle = \langle y_0y'_0\rangle = 0$ in the middle of the quadrupoles. The matched rms beam size at $z=0$ in the middle of a quadrupole is

$$\sigma_x^2 = 2\epsilon|f|\sqrt{\frac{2f+L}{2f-L}}, \qquad \sigma_y^2 = 2\epsilon|f|\sqrt{\frac{2f-L}{2f+L}}, \quad (6)$$

where L is the FODO lattice half-period, approximately equal to the single undulator module length, and ϵ is the

transverse geometric emittance, typically the same in both dimensions. The lattice must satisfy $L < 2|f|$. The rms divergence in x and y may be calculated from the geometric emittance $\sigma_{x'} = \epsilon/\sigma_x$, $\sigma_{y'} = \epsilon/\sigma_y$.

In experiments at LCLS, a reverse-tapered [23] undulator upstream of the Delta undulator produces a highly microbunched beam with minimal background radiation. We therefore expect $E_\nu(\boldsymbol{\phi}; 0) \approx 0$ in Eq. (2). The Delta undulator is only one or two gain lengths long, so we ignore the FEL interaction and hence the right side of Eq. (2). While this assumption removes self-consistency from Eqs. (1) and (2), it leads to an expression that may be compared with experiment and simulation. With this assumption, Eq. (2) can be solved to give

$$F_\nu = F_\nu(\mathbf{x}_0, \mathbf{x}_0', \eta; 0) \exp\left(-2ik_u z\eta\nu + ikz\,\mathbf{x}'^2/2\right), \tag{7}$$

where $\mathbf{x}'$ is the z derivative of Eqs. (3) and (4). If $\mathbf{x}_0$, $\mathbf{x}_0'$, and η are independent and normally distributed,

$$F_\nu(\mathbf{x}_0, \mathbf{x}_0', \eta; 0) \propto b_\nu(\mathbf{x}_0; 0) \times \exp\left(-\frac{x_0^2}{2\sigma_x^2} - \frac{y_0^2}{2\sigma_y^2} - \frac{x_0'^2}{2\sigma_{x'}^2} - \frac{y_0'^2}{2\sigma_{y'}^2} - \frac{\eta^2}{2\sigma_\eta^2}\right), \tag{8}$$

where σ_η is the rms energy spread. After a change of variables equivalent to an application of Liouville's theorem, the right side of Eq. (1) becomes

$$\int d\mathbf{x}' d\eta \tilde{F}_\nu = \int d\mathbf{x}_0' d\eta d\mathbf{x}_0 e^{-ik\mathbf{x}\cdot\boldsymbol{\phi}} F_\nu = b_\nu(\boldsymbol{\phi}; z). \tag{9}$$

Equation (9) can be integrated exactly with the integrand given by Eqs. (7) and (8). The result generalizes expressions seen elsewhere [16,17,24–26] to include the effects of quadrupole focusing, emittance, and energy spread for a matched beam,

$$b_\nu(\phi_x = 0, \phi_y; z) = \frac{b_\nu(\phi_x = 0, \phi_y; 0)}{i + 2\hat{\epsilon}|\hat{z}|/\sqrt{1-\hat{L}^2}} \times \exp\left(-2(k_u\sigma_\eta\nu z)^2 + |f|k\frac{i\psi + \zeta}{\sqrt{1-\hat{L}^2} - 2i\hat{\epsilon}|\hat{z}|}\right), \tag{10}$$

where $\hat{L} = L/2f$, $\hat{z} = z/2f$, $\hat{\epsilon} = \epsilon k$,

$$\psi = |\hat{z}|\sqrt{1-\hat{L}^2}(\alpha^2 - 2\alpha\phi_y + \phi_y^2\hat{\epsilon}^2),$$
$$\zeta = -\hat{\epsilon}\phi_y[(1-\hat{L})(\phi_y - 2\alpha\hat{z} + 2\phi_y\hat{z}) + 2\phi_y\hat{z}^2],$$

and $\phi_x = 0$ for brevity. The $\phi_x \neq 0$ behavior may be recovered by setting α to zero, negating f, and changing ϕ_y to ϕ_x.

The angle at which $|b_\nu(\phi_y; z)|^2$ reaches a maximum is α_b. After squaring Eq. (10) and differentiating with respect to ϕ_y we find

$$\alpha_b(\hat{z}) = \alpha\hat{z}\frac{1}{1 - 2\hat{z}\frac{\hat{L} - \hat{z} - \hat{z}\hat{\epsilon}^2}{1-\hat{L}+2\hat{z}}}. \tag{11}$$

Equation (11) can be simplified when the emittance is small and the quad separation is larger than $2f$,

$$\hat{\epsilon}^2\hat{L}^2 \ll 1 - \hat{L}^2. \tag{12}$$

Condition (12) is hardly a constraint, for most FELs satisfy $\hat{\epsilon} < 1/2$ by design, and $\hat{L}$ is kept well below unity to optimize the gain length. With Eq. (12) satisfied, the microbunch angle after a single undulator drift $\hat{z} = \hat{L}$ matches the first term in Eq. (5),

$$\alpha_b(\hat{z} = \hat{L}) \approx \alpha\hat{L} = \frac{\alpha L}{2f}. \tag{13}$$

Evidently the microbunches rotate toward (away from) the kick direction after passing through a defocusing (focusing) quadrupole. This microbunch rotation can help or hinder off-axis lasing. The magnitude of the rotation can approach the kick angle. This effect is entirely geometric—no gain is needed to explain the microbunch rotation.

This rotation comes at a cost, however. During the microbunch rotation, the smearing and curvature terms in Eq. (5) degrade the bunching. The bunching magnitude at the angle specified by Eq. (11) is

$$|b_\nu(\phi_x = 0, \phi_y = \alpha_b; z)|^2 \propto e^{-\alpha^2/\alpha_c^2},$$

where the critical angle α_c is given by

$$\alpha_c^2|f|k = \frac{\hat{\epsilon}}{\sqrt{1-\hat{L}^2}} + \frac{1 - 2\hat{L}\,\hat{z} - \hat{L} + 2\hat{z}^2 + 2\hat{z}}{2\hat{\epsilon}\hat{z}^2\sqrt{1-\hat{L}^2}}. \tag{14}$$

This is a generalized version of the critical angle discussed in [16]. The second term is typically dominant, highlighting the importance of a small emittance. Again applying Eq. (12), α_c reduces to

$$\alpha_c(\hat{z} = \hat{L})^2 \approx \frac{1}{2|f|k\hat{\epsilon}\hat{L}^2}\sqrt{\frac{1+\hat{L}}{1-\hat{L}}} = \frac{1}{k^2\hat{L}^2\sigma_y^2}, \tag{15}$$

where σ_y is the beam size in the middle of the quadrupole, Eq. (6). The importance of microbunch tilt can be estimated by calculating the tilt when the beam is kicked at the critical angle. If the condition in Eq. (12) is met, the result is

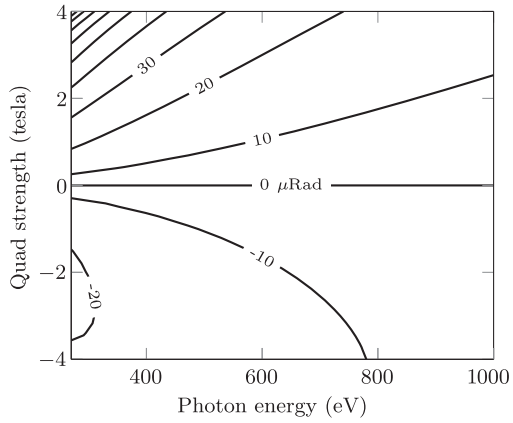

FIG. 2. The microbunch tilt angle $\alpha_b(\hat{z}=\hat{L},\alpha=\alpha_c)$ (in μRad) is plotted as a function of photon energy and integrated quadrupole strength using the LCLS beam and lattice parameters. The kick angle α is chosen to be the critical angle, Eq. (15), and the drift length is $\hat{z}=\hat{L}$. At LCLS the integrated quadrupole strength can vary from −4 to 4 T, and the photon energy can reach down to 270 eV.

$$\alpha_b(\hat{z}=\hat{L},\alpha=\alpha_c)\approx\frac{1}{k\sigma_y}\frac{f}{|f|}. \tag{16}$$

Equation (16) is plotted in Fig. 2 as a function of photon energy and quadrupole strength for LCLS-like parameters. In this figure quadrupole strength refers to the quadrupole gradient integrated along the central axis.

The microbunch angle in Eq. (16) can exceed the coherent undulator radiation divergence $\sigma_{r'}\approx\sqrt{\pi/kL}$. When it does, microbunch rotation is expected to have an effect on the radiation produced by a kicked beam.

III. COHERENT RADIATION FROM A KICKED BEAM

The electric field may be calculated numerically from Eq. (1), but more physical insight can be gained through approximation. At LCLS the energy spread before saturation satisfies

$$2(k_u\sigma_\eta z)^2\ll 1. \tag{17}$$

Henceforth, we assume Eqs. (12) and (17) are satisfied.

Equation (1) can be rewritten with the relabeling $\tilde{E}_\nu(\boldsymbol{\phi};z)\to\exp(i\Delta\nu k_u z+\frac{1}{2}ik\boldsymbol{\phi}^2 z)\tilde{E}_\nu(\boldsymbol{\phi};z)$ as

$$\frac{\partial\tilde{E}_\nu}{\partial z}\propto b_\nu(\boldsymbol{\phi};z)e^{i\Delta\nu k_u z+\frac{1}{2}ik\boldsymbol{\phi}^2 z}. \tag{18}$$

This is valid because $(\Delta\nu k_u+k\boldsymbol{\phi}^2/2)$ is independent of z in the Delta undulator, and an overall phase will not affect $|E|^2$.

Inserting Eq. (10) into Eq. (18) and applying Eq. (12), the resultant expression for the field growth is

$$\frac{\partial\tilde{E}_\nu}{\partial z}\propto\exp\left\{-\frac{\alpha^2}{2\alpha_c^2}-\frac{1}{2}k^4z^2\varepsilon^2\alpha_c^2(\phi_y-\alpha_b)^2+i[k_u\Delta\nu+k\frac{(\alpha-\phi_y)^2}{2}]z\right\}, \tag{19}$$

where α_b and α_c are Eqs. (11) and (14) subject to Eq. (12).

Equation (19) may be integrated with respect to z, but the result involves error functions, and cannot be written compactly. In lieu of additional approximations we discuss the maximization of $|\tilde{E}_\nu|^2$ through the minimization of the factors in the exponent of $\partial\tilde{E}_\nu/\partial z$.

There is an unavoidable field degradation when α approaches α_c. This is a consequence of microbunch smearing. The $(\phi_y-\alpha_b)^2$ dependence indicates a tendency to radiate perpendicular to the microbunches, while the $(\alpha-\phi_y)^2$ dependence indicates a tendency to emit along the new travel direction.

Fortunately, the microbunches can rotate toward the new travel direction, so the field growth is strongest when $\phi_y=\alpha_b$ and

$$\Delta\nu=-k(\alpha-\alpha_b)^2/(2k_u).$$

This can be converted into a detune in undulator K by noting that the beam will radiate at a wave number k set by the premicrobunched beam,

$$\frac{\Delta K}{K_0}\approx-\frac{k(\alpha-\alpha_b)^2}{4k_u},$$

where K_0 is the rms undulator parameter resonant to the premicrobunched beam with zero kick. This detune is a moving target, since the microbunch angle α_b changes as the beam propagates. The exact optimal detune must be calculated numerically by integrating Eq. (19), but the rotation of the microbunches serves to move the optimal detune closer to zero when $f>0$. For $f<0$, the rotating microbunches move away from the kick direction, thus moving the optimal detune farther away from 0.

This can be contrasted with a formalism developed without microbunch rotation, $\alpha_b=0$ [16,17], and with a formalism with immediate rotation, $\alpha_b=\alpha$. We therefore seek evidence of steady rotation in the next section.

IV. SIMULATION AND EXPERIMENT

The microbunch tilt at LCLS is expected to be most pronounced in the soft x-ray region, so we compare the predictions of the previous section with data acquired during a 530 eV experiment and matching GENESIS simulations. A list of lattice and beam parameters may be found in Table I.

Microbunch tilt can be directly observed in simulation, as seen in Fig. 3(a). Here, an electron density map from a single slice of a time-dependent GENESIS [27] simulation is shown to display a substantial tilt upward. Simulation parameters match Table I, and the kick supplied was

TABLE I. LCLS undulator lattice and beam parameters used for the 530 eV experiment and simulations.

Parameter	Symbol	Value
Quadrupole strength (T)		3.0
Quadrupole focal length (m)	f	3.84
Quadrupole spacing (m)	L	3.9
Undulator period (cm)	λ_u	3.0
Undulator rms K value	K	2.47[a]
Undulator length (m)		3.3
Beam energy (GeV)	γmc^2	3.43
Normalized emittance (μm)	$\gamma\epsilon$	0.4[b]
RMS energy spread (MeV)	$\gamma mc^2\sigma_\eta$	3.0[b]
Peak current (kA)	I	3.0

[a]K varies slightly in the reverse taper and Delta.
[b]Typical value under these conditions, not measured.

$\alpha = 55$ μRad. The slice density is plotted at the end of the undulator, 3.6 m away from the middle of the quadrupole centered at $z = 0$. The microbunch tilt can be calculated as the angle at which $|b(\boldsymbol{\phi})|^2$ reaches a maximum value. This angle is plotted as a function of z and compared with Eq. (11) in Fig. 3(b).

In these simulations we reproduce experimental conditions as closely as possible. A linearly polarized photon pulse and the electron beam are extracted from a six-segment-long reverse-tapered undulator line. These beams are then sent into a circularly polarized Delta undulator. The Delta in these simulations is coaxial with the reverse-tapered undulators, matching experiment. The electron beam is kicked steadily over the 0.3-m-long quadrupole upstream of the Delta. The linearly polarized background radiation is decomposed into left and right circular components, only one of which interacts in the Delta. In Fig. 3 the undulator is set to a K that maximizes the output power.

The K at which the power reaches a maximum value offers an indirect measure of the microbunch tilt. In Fig. 4 we calculate the predicted detune from Eq. (19), and compare with simulation and experiment. We also calculate the detune predicted from Eq. (19) under the assumption that $\alpha_b = 0$, namely, $\Delta\nu = -k\alpha^2/(2k_u)$. The theoretical curves use Table I parameters. For ease of integration

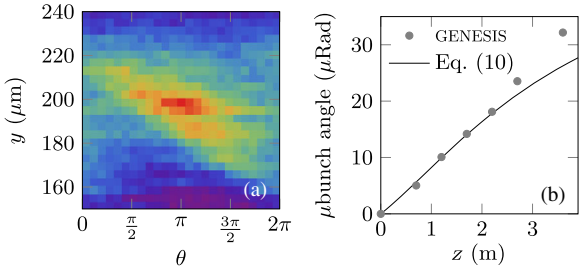

FIG. 3. (a) A slice of the output beam from a GENESIS simulation following a 55 μRad kick. θ is the ponderomotive phase. (b) The angle of maximum bunching is plotted against Eq. (11) at several positions along the undulator.

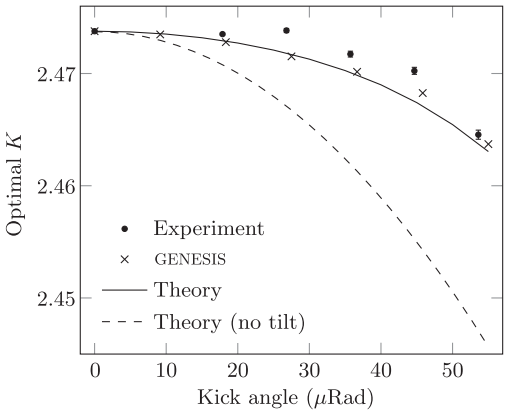

FIG. 4. The undulator rms K that yields the largest power is plotted as a function of kick angle. Data collected at LCLS (solid circles), GENESIS simulations (crosses), theory with rotation (solid line), and theory without rotation (dashed line).

the undulator length is chosen to be the lattice half-period 3.9 m. The experimental data are derived from a gas detector which has a wider acceptance angle than downstream screens. A 30% roll-off in efficiency is observed at the greatest spot separation, but this roll-off is not expected to impact the optimal K calculation since the optimal K produces minimal downstream spot separation.

One of the primary benefits of microbunch rotation is that the electron beam radiates more efficiently off axis. In Fig. 5(a) we show the radiation distribution on a yttrium-aluminium-garnet (YAG) screen 87 m downstream from the Delta undulator. The electron beam kick was $\alpha = 55$ μRad, and the measured radiation displacement of the circularly polarized top spot was calculated to be 35 μRad.

Figure 5(a) shows substantial obstruction of the YAG screen by circular irises. Unfortunately, several of these irises are also upstream of the gas detector, so it is difficult to estimate the total power in the diverted beam. Rather than rely on the obstructed gas detector, we apply a 2D Gaussian fit to each spot on the direct imager. At a K

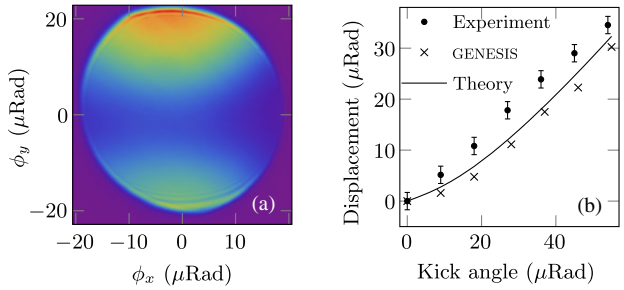

FIG. 5. (a) The measured radiation distribution from a kicked beam lasing in the Delta undulator. Both the background linear light on the bottom and the light from Delta on the top are partially obscured by circular irises. (b) At a fixed K of 2.47325, the radiation displacement angle with different electron beam kicks (solid circles) is compared with simulation (crosses) and theory with rotation (dashed line).

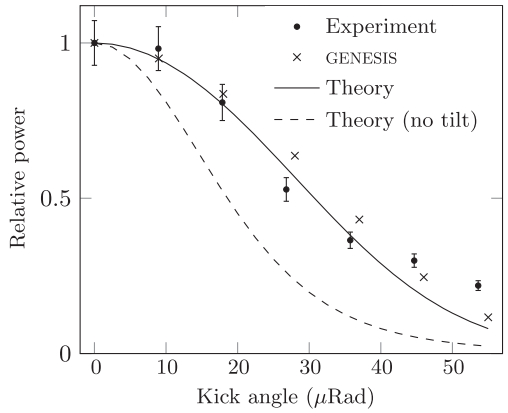

FIG. 6. The integrated off-axis circular spot intensity is plotted against the kick angle. LCLS data (solid circles) and GENESIS results (crosses) are compared with the theory with rotation (solid line) and without rotation (dashed line). The integrated power is calculated from a 2D Gaussian fit to images like the one in Fig. 5(a).

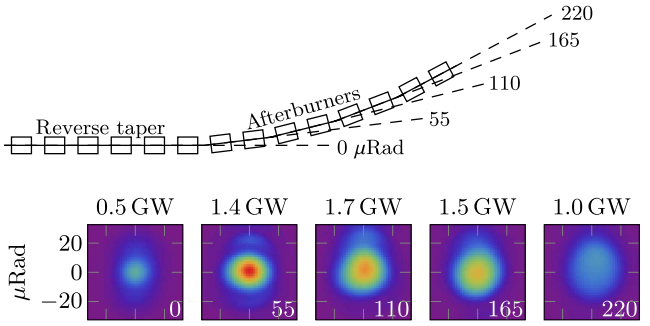

FIG. 7. A simulated electron beam is microbunched in six reverse-tapered undulators, and then diverted four times (top). After each kick, two helical undulators provide a lasing medium. After each two-undulator segment, the output radiation spot is shown in the far field (bottom). The left-to-right ordering of the plots matches the diagram above, and the coordinate system for each plot is recentered to the new beam direction. Thus, the 1.0-GW spot is 220 μRad above the original axis.

of 2.47325, the measured radiation angle displacement is compared with our theory and GENESIS simulations in Fig. 5(b).

In producing Fig. 5(b), a two-dimensional Gaussian distribution was fit to both the linear and the circular spot. The displacement at a kick angle α is the change in the centroid of the circular spot relative to its position at $\alpha = 0$.

Off-axis radiation is expected whether or not the microbunches tilt. The $(\alpha - \phi_y)^2$ dependence of Eq. (19) suggests that an increasing α should naturally lead an increasing angle of maximum emission. However, without microbunch tilt, the intensity of the off-axis radiation will be much lower at the larger kick values as a result of the $(\phi_y - \alpha_b)^2$ dependence of Eq. (19).

This hypothesis is tested in Fig. 6. The same increasing kick at $K = 2.47325$ is applied, but the integrated off-axis spot intensity is plotted instead. Without microbunch tilt, the theory systematically underpredicts the power in the off-axis spot at every kick angle.

The theory with rotation underpredicts the power at large angles. This is likely due to gain effects that are not included in the derivation of Eq. (19). GENESIS simulations with an initial energy spread smaller than the conservative value of Table I also exhibited larger powers at these larger angles.

V. SOFT X-RAY APPLICATIONS

Rotating microbunches are useful for the production of off-axis radiation. Both the on-axis and off-axis spot could serve different users, offering an undulator-based alternative to existing two-experiment multiplexing techniques [28–30]. However, there is no reason to stop at two beams. For example, a simulated five-beam bent FEL is presented in Fig. 7.

In this simulation, a beam and lattice with the parameters given in Table I is repeatedly kicked by 55 μRad upward. After each kick, the simulation coordinate system is rotated by 55 μRad, and the beam is sent through two circularly polarized undulators. The electron beam is transferred from the previous coordinate system to the new coordinate system after each kick. The previous x-ray beam is not transferred, so the result is consistent with an arc composed of pairs of undulators with alternating left and right circular polarization. With a two-undulator drift and carefully chosen detune, the microbunches rotate to be perpendicular to the new direction of travel, and the FEL gain process can make up for microbunch smearing. This gain-assisted multistaged approach permits microbunch rotation through angles far in excess of the critical angle α_c. This bent FEL is limited by normal saturation effects in FELs, though care must be taken to ensure the gain counteracts the smearing and curvature terms in Eq. (5).

The microbunch rotation scheme in Fig. 7 requires only magnetic optics that are already present in an undulator line. This contrasts with the elegant but lengthy achromatic systems envisioned to rotate and preserve microbunches through a bend [15,32,33].

A proof of principle experiment was conducted using planar undulators at 530 eV. Geometric constraints limited the number of visible beams to three, seen in Fig. 8. An undulator configuration of 6 reverse tapered undulators, 2 undulators at 55 uRad, and 3 undulators at 110 uRad was used. Each beam contains 30 μJ, equivalent to an average power of 0.5 GW. GENESIS simulation of a standard SASE FEL shows the power after 3 undulators to be only 8.6 MW, indicating the microbunches are rotating toward the new kick direction following each kick.

Other multiplexing geometries are possible. For example, a horizontal kick following the appropriate quadrupole would permit multiplexing in a two-dimensional

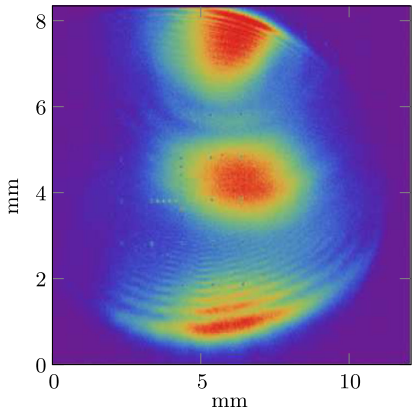

FIG. 8. Three beams from a multiplexed FEL experiment conducted at LCLS. The spot separation is approximately 55 uRad, which manifests as a 3.5 mm spacing on the screen. A triple Gaussian fit and the known YAG response [31] indicate the bottom, middle, and top spots contain 27, 30, and 33 μJ respectively. The bottom spot is clipped and diffracted by the undulator line vacuum chamber.

grid. Alternatively, Eq. (16) shows that large microbunch rotation angles are possible when σ_y is small in a defocusing quadrupole. Where stronger quadrupoles are available and large beam aspect ratios tolerable, microbunches may be preserved through single kicks several hundred μRad in magnitude. Sextupoles may also aid in decreasing microbunch curvature, increasing permitted rotation angles even further [34]. The microbunching wavelength is fixed in Figs. 7 and 8, but emission at the third or fifth harmonic is possible, as is an arbitrary polarization in each pulse.

The scheme in Figs. 7 and 8 uses the fact that microbunches rotate toward the new direction of travel following a defocusing quadrupole. However, with a nonoptimal detune or a focusing quadrupole, a beam can be forced to radiate at an angle not perpendicular to the microbunches. Such a radiator would produce a photon beam whose wave fronts are rotated with respect to the direction of travel, the so-called pulse-front tilted beam [35]. The potential tilt is limited by the exponential suppression of the radiation power by the second term in Eq. (19).

VI. IMPROVED ROTATION AND HARD X RAYS

At hard x-ray wavelengths, increasing the quadrupole strength is not a viable solution. The smearing term $\alpha z y_0'$ and the curvature term $z y_0^2/8f^2$ from Eq. (5) rapidly destroy angstrom-scale microbunches. The result, demonstrated by the wavelength scaling in Eq. (15), is a critical angle of $\sim$2 μRad at 1.5 Å.

Fortunately, there is a periodic magnetic lattice that eliminates the smearing term and minimizes the curvature term. Consider the quadrupole triplet in Fig. 9 with parameters matching Table II. A repetitive lattice composed of 21 of these triplets was once considered as an alternative to a FODO lattice at LCLS [36]. Here, we concentrate on the dynamics of a microbunched beam passing through a single quadrupole triplet.

TABLE II. Triplet lattice and hard x-ray beam parameters.

Parameter	Value
First and third quadrupole gradient (T/m)	240.0
First and third quadrupole length (cm)	6.0
Second quadrupole gradient (T/m)	−240.0
Second quadrupole length (cm)	12.0
Interquad spacing (cm)	6.0
Beam energy (GeV)	13.64[a]
Microbunch wavelength (Å)	1.5
Triplet y offset, first and third quadrupole (mm)	1.0[b]
Triplet y offset, second quadrupole (mm)	0.94[b]

[a]All unlisted beam parameters match Table I.
[b]Measured from beam position at triplet entrance.

In Fig. 9, a large transverse offset between the beam and first quadrupole produces a large upward kick $\alpha > 0$, and a defocusing effect $f > 0$. The result is a tilt in the direction of sign(α/f), the $+y$ direction. The short drift has suppressed the curvature term from Eq. (5). Unfortunately, there is a strong smearing correlation between z and y' in accordance with sign(α) that degrades the microbunching.

The second quadrupole changes the sign of f and α but preserves the magnitude of α. Thus, the tilt continues to grow, but the smearing term $\alpha z y_0'$ from the first drift is canceled by the second drift. The middle quadrupole can be perturbed to align the microbunch normal with the output direction.

The result is a microbunched beam that rotates 20 μRad with less than 1% degradation in $|b|$, as shown in Fig. 10(a). In this figure, an electron beam from a 1.5-Å

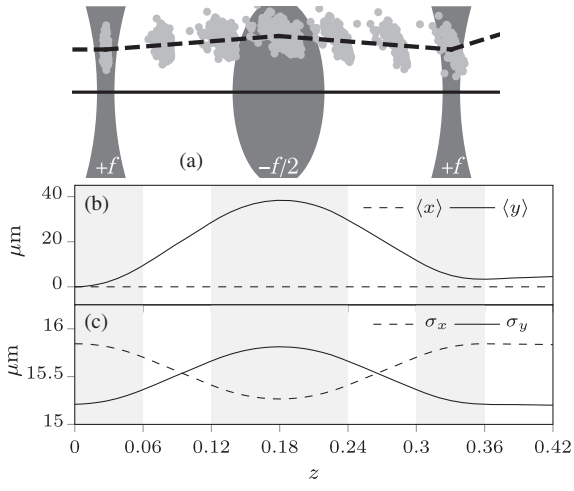

FIG. 9. (a) Microbunched electrons (light gray circles) propagate through a magnetic triplet (dark gray). A transverse offset between the triplet axis and the beam axis provides the trajectory (b) and rms beam size (c) required to rotate bunches and preserve their structure.

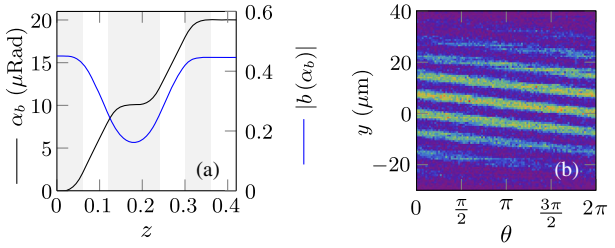

FIG. 10. (a) Microbunch angle (black line) and microbunching magnitude (blue line) evolution in a quadrupole triplet (gray) GENESIS simulation. (b) An electron density map of an output slice at 0.42 m exhibiting 20-μRad upward tilt.

time-dependent GENESIS simulation near saturation is sent through the offset quadrupole triplet of Table II.

The 20-μRad rotation is a factor of 10 greater than α_c at this energy, and it comes without microbunch degradation. An analysis of the limits of this scheme should include higher order correlations and dispersion if the rotation exceeds a few hundred microradians, an exercise that is beyond the scope of this discussion. We also note that 240 T/m is a high gradient for undulator lattices [37], but within the range of commercially available permanent magnet quadrupoles, which have reached 655 T/m [38].

The x-ray FEL oscillator [39,40] can benefit from this rotation scheme [41]. A diverted beam with rotated microbunches provides a way for an electron beam from the oscillator cavity to continue radiating off axis, avoiding damage to the cavity mirrors and increasing the output power.

The multiplexing scheme of Fig. 7 can also be improved by replacing the FODO lattice with a triplet lattice. A heavily multiplexed FEL may find relevance in the photolithography industry, where a reliable 13.5-nm source remains elusive. The offset quadrupole triplet may also play a role in the development of a ring FEL.

VII. CONCLUSION

We have presented experimental evidence that microbunches can rotate toward the new direction of travel when the electron beam is simultaneously diverted and defocused. We have developed a theory to explain the source of this rotation, and compared it with data collected during the commissioning of the Delta undulator at LCLS, and with time-dependent GENESIS simulations.

Rotating microbunches are a new tool for accelerator physicists, enabling off-axis lasing, improved multiplexing, beams with a pulse-front tilt, and microbunch preservation through a bend. We demonstrate that these applications are available at soft x-ray FELs.

We have applied this understanding to a more optimized magnetic system—the offset quadrupole triplet—capable of rotating microbunches without measurable degradation. Preservation of angstrom-scale beam structure through a rotation extends these new applications from the soft x-ray to any accessible wavelength.

ACKNOWLEDGMENTS

This work is supported by DOE Contract No. DE-AC02-76SF00515 and the Robert Siemann Graduate Fellowship. The authors thank K.-J. Kim, H.-D. Nuhn, E. A. Schneidmiller, A. Marinelli, G. Stupakov, B. Fawley, R. Lindberg, R. A. Lai, G. Geloni, E. Saldin, and H. Braun for fruitful discussions.

[1] C. Pellegrini, A. Marinelli, and S. Reiche, *The Physics of X-Ray Free-Electron Lasers*, Rev. Mod. Phys. **88**, 015006 (2016).

[2] C. Bostedt, S. Boutet, D. M. Fritz, Z. Huang, H. J. Lee, H. T. Lemke, A. Robert, W. F. Schlotter, J. J. Turner, and G. J. Williams, *Linac Coherent Light Source: The First Five Years*, Rev. Mod. Phys. **88**, 015007 (2016).

[3] E. L. Saldin, E. A. Schneidmiller, and M. V. Yurkov, *Self-Amplified Spontaneous Emission FEL with Energy-Chirped Electron Beam and Its Application for Generation of Attosecond X-Ray Pulses*, Phys. Rev. ST Accel. Beams **9**, 050702 (2006).

[4] A. A. Zholents, *Method of an Enhanced Self-Amplified Spontaneous Emission for X-Ray Free Electron Lasers*, Phys. Rev. ST Accel. Beams **8**, 040701 (2005).

[5] G. Penco, E. Allaria, I. Cudin, S. Di Mitri, D. Gauthier, S. Spampinati, M. Trovó, L. Giannessi, E. Roussel, S. Bettoni *et al.*, *Passive Linearization of the Magnetic Bunch Compression Using Self-Induced Fields*, Phys. Rev. Lett. **119**, 184802 (2017).

[6] T. Hara, C. Kondo, T. Inagaki, K. Togawa, K. Fukami, S. Nakazawa, T. Hasegawa, O. Morimoto, M. Yoshioka, H. Maesaka *et al.*, *High Peak Current Operation of X-Ray Free-Electron Laser Multiple Beam Lines by Suppressing Coherent Synchrotron Radiation Effects*, Phys. Rev. Accel. Beams **21**, 040701 (2018).

[7] M. W. Guetg, A. A. Lutman, Y. Ding, T. J. Maxwell, F.-J. Decker, U. Bergmann, and Z. Huang, *Generation of High-Power High-Intensity Short X-Ray Free-Electron-Laser Pulses*, Phys. Rev. Lett. **120**, 014801 (2018).

[8] A. Marinelli, D. Ratner, A. Lutman, J. Turner, J. Welch, F.-J. Decker, H. Loos, C. Behrens, S. Gilevich, A. Miahnahri *et al.*, *High-Intensity Double-Pulse X-Ray Free-Electron Laser*, Nat. Commun. **6**, 6369 (2015).

[9] E. Prat, F. Löhl, and S. Reiche, *Efficient Generation of Short and High-Power X-Ray Free-Electron-Laser Pulses Based on Superradiance with a Transversely Tilted Beam*, Phys. Rev. ST Accel. Beams **18**, 100701 (2015).

[10] A. A. Lutman, T. J. Maxwell, J. P. MacArthur, M. W. Guetg, N. Berrah, R. N. Coffee, Y. Ding, Z. Huang, A. Marinelli, S. Moeller *et al.*, *Fresh-Slice Multicolour X-Ray Free-Electron Lasers*, Nat. Photonics **10**, 745 (2016).

[11] A. A. Lutman, J. P. MacArthur, M. Ilchen, A. O. Lindahl, J. Buck, R. N. Coffee, G. L. Dakovski, L. Dammann, Y. Ding, H. A. Dürr *et al.*, *Polarization Control in an X-Ray Free-Electron Laser*, Nat. Photonics **10**, 468 (2016).

[12] D. J. Higley, K. Hirsch, G. L. Dakovski, E. Jal, E. Yuan, T. Liu, A. A. Lutman, J. P. MacArthur, E. Arenholz, Z. Chen *et al.*, *Femtosecond X-Ray Magnetic Circular Dichroism Absorption Spectroscopy at an X-Ray Free Electron Laser*, Rev. Sci. Instrum. **87**, 033110 (2016).

[13] G. Hartmann, A. Lindahl, A. Knie, N. Hartmann, A. Lutman, J. MacArthur, I. Shevchuk, J. Buck, A. Galler, J. Glownia *et al.*, *Circular Dichroism Measurements at an X-Ray Free-Electron Laser with Polarization Control*, Rev. Sci. Instrum. **87**, 083113 (2016).

[14] N. Gavrilov, G. Kulipanov, V. Litvinenko, I. Pinayev, V. Popik, I. Silvestrov, A. Skrinsky, A. Sokolov, N. Vinokurov, and P. Vobly, *Observation of Mutual Coherence of Spontaneous Radiation from Two Undulators Separated by an Achromatic Bend*, Nucl. Instrum. Methods Phys. Res., Sect. A **304**, 63 (1991).

[15] Y. Li, W. Decking, B. Faatz, and J. Pflueger, *Microbunch Preserving Bending System for a Helical Radiator at the European X-Ray Free Electron Laser*, Phys. Rev. ST Accel. Beams **13**, 080705 (2010).

[16] T. Tanaka, H. Kitamura, and T. Shintake, *Consideration on the BPM Alignment Tolerance in X-Ray FELs*, Nucl. Instrum. Methods Phys. Res., Sect. A **528**, 172 (2004).

[17] G. Geloni, V. Kocharyan, and E. Saldin, *On Radiation Emission from a Microbunched Beam with Wave Front Tilt and Its Experimental Observation*, Opt. Commun. **410**, 180 (2018).

[18] G. Geloni, V. Kocharyan, and E. Saldin, *Evidence of Wigner Rotation Phenomena in the Beam Splitting Experiment at the LCLS*, arXiv:1607.02928.

[19] G. Geloni, V. Kocharyan, and E. Saldin, *Misconception Regarding Conventional Coupling of Fields and Particles in XFEL Codes*, arXiv:1601.07738.

[20] G. Geloni, V. Kocharyan, and E. Saldin, *Effect of Aberration of Light in X-Ray Free Electron Lasers*, arXiv:1511.01375.

[21] K.-J. Kim, Z. Huang, and R. Lindberg, *Synchrotron Radiation and Free-Electron Lasers* (Cambridge University Press, Cambridge, England, 2017).

[22] A. Chao, K. Mess, M. Tigner, and F. Zimmermann, *Handbook of Accelerator Physics and Engineering*, 2nd ed. (World Scientific, Singapore, 2013), pp. 543–765.

[23] E. A. Schneidmiller and M. V. Yurkov, *Obtaining High Degree of Circular Polarization at X-Ray Free Electron Lasers via a Reverse Undulator Taper*, Phys. Rev. ST Accel. Beams **16**, 110702 (2013).

[24] K.-J. Kim, M. Xie, and C. Pellegrini, *Effects of Undulator Interruptions on the Performance of High-Gain FEL Amplifiers*, Nucl. Instrum. Methods Phys. Res., Sect. A **375**, 314 (1996).

[25] K.-J. Kim, *Undulator Interruption in High-Gain Free-Electron Lasers*, Nucl. Instrum. Methods Phys. Res., Sect. A **407**, 126 (1998).

[26] P. Baxevanis, Z. Huang, and G. Stupakov, *Effect of an Angular Trajectory Kick in a High-Gain Free-Electron Laser*, Phys. Rev. Accel. Beams **20**, 040703 (2017).

[27] S. Reiche, *GENESIS 1.3: A Fully 3D Time-Dependent FEL Simulation Code*, Nucl. Instrum. Methods Phys. Res., Sect. A **429**, 243 (1999).

[28] Y. Feng, R. Alonso-Mori, T. Barends, V. Blank, S. Botha, M. Chollet, D. Damiani, R. B. Doak, J. Glownia, J. Koglin *et al.*, *Demonstration of Simultaneous Experiments Using Thin Crystal Multiplexing at the Linac Coherent Light Source*, J. Synchrotron Radiat. **22**, 626 (2015).

[29] T. Plath, P. Amstutz, J. Boedewadt, G. Brenner, N. Ekanayake, B. Faatz, K. Hacker, K. Honkavaara, L. L. Lazzarino, C. Lechner *et al.*, *Free-Electron Laser Multiplex Driven by a Superconducting Linear Accelerator*, J. Synchrotron Radiat. **23**, 1070 (2016).

[30] S. Boutet, L. Foucar, T. R. Barends, S. Botha, R. B. Doak, J. E. Koglin, M. Messerschmidt, K. Nass, I. Schlichting, M. M. Seibert *et al.*, *Characterization and Use of the Spent Beam for Serial Operation of LCLS*, J. Synchrotron Radiat. **22**, 634 (2015).

[31] J. Krzywinski, A. Andrejczuk, R. M. Bionta, T. Burian, J. Chalupsky, M. Jurek, M. Kirm, V. Nagirnyi, R. Sobierajski, K. Tiedtke, S. Vielhauer, and L. Juha, *Saturation of a Ce:* $Y_3Al_5O_{12}$ *Scintillator Response to Ultra-Short Pulses of Extreme Ultraviolet Soft X-Ray and X-Ray Laser Radiation*, Opt. Mater. Express **7**, 665 (2017).

[32] K. L. Brown, *A Second-Order Magnetic Optical Achromat*, IEEE Trans. Nucl. Sci. **26**, 3490 (1979).

[33] N. Vinokurov, *Multisegment Wigglers for Short Wavelength FEL l*, Nucl. Instrum. Methods Phys. Res., Sect. A **375**, 264 (1996).

[34] H. Braun (private communication).

[35] S. Akturk, X. Gu, P. Gabolde, and R. Trebino, *The General Theory of First-Order Spatio-Temporal Distortions of Gaussian Pulses and Beams*, Opt. Express **13**, 8642 (2005).

[36] P. Emma and H.-D. Nuhn, *Quadrupole Magnet Error Sensitivities for FODO-Cell and Triplet Lattices in the LCLS Undulator*, LCLS Technical Report No. 10.2172/839698 (2000).

[37] I. Okunev, I. Morozov, and N. Nefedov, *X-FEL Quadrupole with Gradient of* 100 T/m, Phys. Procedia **84**, 101 (2016).

[38] K. Nakamura, T. Sokollik, J. van Tilborg, A. J. Gonsalves, B. Shaw, S. Shiraishi, R. Mittal, S. De Santis, J. M. Byrd, and W. Leemans, *Beam Transport and Monitoring for Laser Plasma Accelerators*, AIP Conf. Proc. **1507**, 728 (2012).

[39] K.-J. Kim, Y. Shvyd'ko, and S. Reiche, *A Proposal for an X-Ray Free-Electron Laser Oscillator with an Energy-Recovery Linac*, Phys. Rev. Lett. **100**, 244802 (2008).

[40] R. R. Lindberg, K.-J. Kim, Y. Shvydko, and W. M. Fawley, *Performance of the X-Ray Free-Electron Laser Oscillator with Crystal Cavity*, Phys. Rev. ST Accel. Beams **14**, 010701 (2011).

[41] K.-J. Kim (private communication).